Static model of a violin bow: influence of camber and hair tension on mechanical behavior

Frédéric Ablitzer, Jean-Pierre Dalmont, Nicolas Dauchez

Static model of a violin bow: influence of camber and hair tension on mechanical behavior

Frédéric Ablitzer[a)] and Jean-Pierre Dalmont

Laboratoire d'Acoustique de l'Université du Maine (UMR CNRS 6613)

avenue Olivier Messiaen,

72085 LE MANS Cedex 9,

France

Nicolas Dauchez

Laboratoire d'Ingénierie des Systèmes Mécaniques et des Matériaux

Supméca,

3 rue Fernand Hainaut,

93407 ST OUEN Cedex,

France

(Dated: April 18, 2011)

Abstract

Experienced bow makers empirically know the influence of wood, tapering and camber on the playing and tonal qualities of a bow. However, the way each parameter affects the bow mechanical behavior is not clearly established. An in-plane finite element model is developed to highlight the link between the adjustable design parameters and the mechanical behavior of a bow. This model takes into account geometric nonlinearity as well as compliance of the hair. Its validity is discussed from measurements on a bow. Results from simulations are compared to experimental results from previous studies. The consequences of adjusting hair tension and camber are then investigated.

PACS numbers: 43.75.De

I. INTRODUCTION

In spite of an extensive scientific literature about the violin[1,2], only few studies are exclusively devoted to the bow. However, experienced players attach almost as much importance to the choice of a bow as to the choice of a violin. They generally asses the quality of a bow in terms of playing and tonal qualities. Playing qualities refer to the control of bow in playing, tonal qualities to the influence on the tone. The question of a link between physical properties and quality of bows was addressed by several authors[3–10]. Static properties such as total mass, mass distribution, and bending stiffness, have generally been assumed to affect the playing qualities, while dynamic properties such as hair and stick modes would relate to the tonal qualities[5,6,11]. In most studies, some static and dynamic properties were measured on different bows with various degrees of quality. Despite the seeming simplicity of the bow compared to the violin, these studies showed that it is not yet possible to predict the quality of a bow by measuring a set of physical properties. However, some authors pointed out the plausible existence of an acceptable range for certain characteristics, out of which the bow would be considered as not suitable for playing[4,6].

When manufacturing a bow stick, the bow maker works with three main parameters: wood, tapering and camber[12]. Regarding wood, high quality modern bows are made of pernambuco (*Caesalpinia Echinata*), a Brazilian wood with high specific Young's modulus and low damping. However, this species has become rare and expensive. Tapering denotes the gradually decreasing thickness along the stick. In general, the maker adjusts the taper of the bow in order to reach the desired total mass, for a given wood density. Camber is the concave curvature of the stick without hair tension. It is adjusted by heating a short portion of the stick over a flame and bending it until it cools down. Once a bow is finished, the only possible adjustment by the player is the hair tension.

This paper aims at highlighting the link between the adjustable design parameters and the mechanical behavior of a bow. Emphasis is put on camber and hair tension, since both

[a)]Electronic address: `frederic.ablitzer.etu@univ-lemans.fr`

can be adjusted on a finished bow. For this purpose, an in-plane finite element model is developed and validated from measurements on bow. It is then used to investigate the effects of hair tension and camber on the mechanical behavior of a standard bow.

II. MODEL OF THE ASSEMBLED BOW

In previous work, various ways of modeling a bow have been proposed. Wegst and Ashby[13] made simple calculation from beam theory, considering a stick with a circular cross-section of constant radius, to determine a typical range of Young's modulus required for violin bows. Pitteroff[14] proposed an analytical model aimed at describing the static behavior of the assembled bow, i.e. stick and hair, in the perpendicular plane. Despite rather rough approximations, the model agreed well with experimentally observed behavior for moderate bow forces. In his model, the stick was represented by its stiffness at the end, which can be written analytically in the case of a simplified geometry. To take into account a more realistic geometry, other authors employed numerical models. Carlsson and Tinnsten[15] used a finite element model coupled to an optimization algorithm to calculate the change in diameter along the stick needed to recover some of the static and dynamic properties after changing density and Young's modulus. The properties of the tightened bow were not investigated in this study.

Caussé *et al.*[7] made simulations based on the finite element model of an assembled bow to highlight mode shapes of stick and hair and to evaluate the influence of hair tension on corresponding eigenfrequencies. In their study, the stress field due to hair tension was taken into account to determine the eigenmodes. This was done in a similar way as Mamou-Mani *et al.*[16] studied the effect of downbearing on piano soundboard eigenfrequencies, but the geometrically nonlinear nature of the problem was not discussed in the case of the bow.

However, the change in geometry during the loading of the bow, e.g. when tightening the hair, is strong enough to cause geometric nonlinearity, even under hypothesis of small deformation and linear behavior of the material, as pointed out by Dauchez *et al.*[8]. In

the present paper, a finite-element model of the bow including the hair and taking into account geometric nonlinearity is now developed. As a starting point, only the in-plane static behavior of the bow is considered.

A. General description

The bow as we know it today is the result of a progressive evolution through centuries[17,18]. Renaissance bows had a short thick stick with convex curvature. As the musical style changed, the stick got longer and thinner, while its curvature was progressively changed from convex to concave in order to withstand the hair tension without increasing the mass too much. At the beginning of the 19th century, the french bow maker François-Xavier Tourte brought the last significant improvements to the design of bows. Today he is considered the father of the modern bow.

A modern violin bow is represented in Figure 1. The stick is traditionnally made of wood. Its main function is to support a 65 cm hair ribbon under tension. The hair is attached to the head of the stick at one end, and to the frog at the other. The hair enters the head through a thin plate, traditionally made of ivory, which covers the underside of the head. The position of the frog is adjusted by turning the button, which operates on a screw mechanism located inside the stick. This allows the player to tighten the hair to suitable tension for playing. The right tension is essentially determined by the transverse compliance of the hair. If too loose, the hair tends to touch the stick in playing. If too tight, more effort is needed to make the string vibrate, according to players and bow makers[19,20]. On early bows, the frog was simply wedged between stick and hair. The resulting hair tension was determined by the height of the frog and the length of the loose hair, both fixed by the bow maker.

The model presented in this paper allows one to simulate, first, the tightening of the bow from its initial state without hair tension [Fig. 2(a)] to its playing state at hair tension T_0 [Fig. 2(b)]; then, the loading by a normal force $\mathbf{F}$. At this step, the hair tension T may

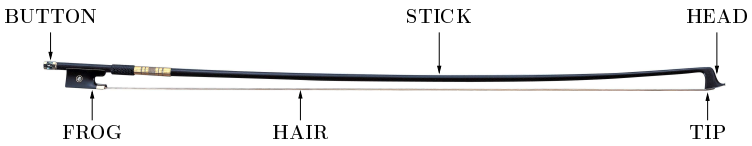

FIG. 1. Modern violin bow.

differ from the initial hair tension T_0 [Fig. 2(c)]. Throughout the simulation, the stick is clamped at the frog end ($x = 0$ mm) and free at the other end.

The model just described is a simplified representation of actual playing conditions. In reality, the bow is held in a finger grip which allows the pivoting around an axis located somewhere near the cut up in the frog, at the position of the thumb. The normal force at the contact point between the hair and the string is controlled by applying a moment with the index finger on top of the stick, with the thumb acting as a support. Since the combined action of index and thumb fingers takes place near the frog, on a thick part of the stick, it is assumed that this modeling makes little difference with the actual static behavior of the bow in playing.

The model takes into account the geometric nonlinearity of the bow as well as the compliance of the hair. It is based on a finite element formulation coupled with an iterative procedure.

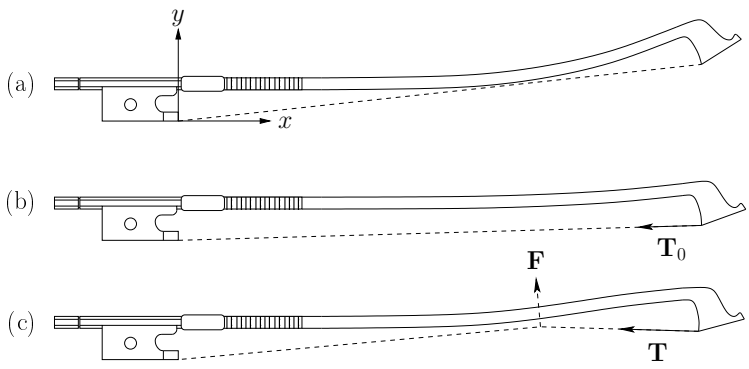

FIG. 2. Bow without tension (a), tightened (b) and loaded (c).

B. Finite element model of the bow

In order to take into account the geometric nonlinearity, the model is based on the corotational formulation for beams given by Crisfield[21]. The corotational formulation allows the global displacements and rotations of a structure to be arbitrarily large, although the local strain are assumed to remain small (Fig. 3). A local reference frame is attached to each element and continuously rotates and translates with it. With respect to this local frame a small-strain, small-displacement relationship is applied. Since a bow stick is slender, this relationship can be derived from the Euler-Bernoulli beam theory.

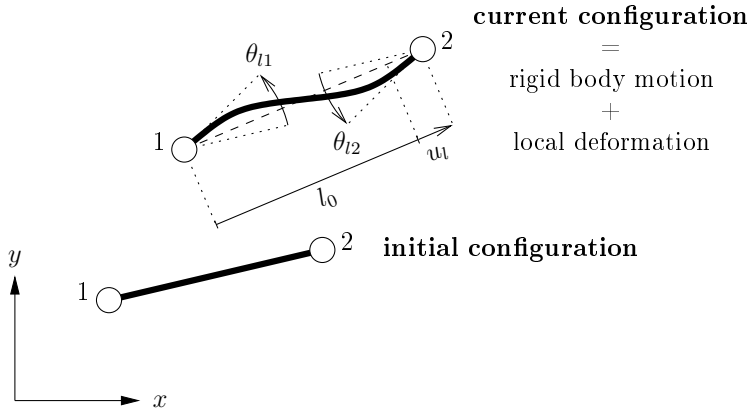

FIG. 3. Initial and current configurations of a beam element.

For each beam element, the axial force N is related to the local axial displacement u_l by the relation

$$N = E\,A\,\frac{u_l}{l_0}\ , \tag{1}$$

where E is the element Young's modulus, A the element area and l_0 the element initial length. The internal bending moments $\bar{M}_1$ and $\bar{M}_2$ are related to the local nodal rotations θ_{l1} and θ_{l2} by the relation

$$\begin{Bmatrix} \bar{M}_1 \\ \bar{M}_2 \end{Bmatrix} = \frac{E\,I}{l_0} \begin{bmatrix} 4 & 2 \\ 2 & 4 \end{bmatrix} \begin{Bmatrix} \theta_{l1} \\ \theta_{l2} \end{Bmatrix}\ , \tag{2}$$

where I is the element second moment of inertia.

The original formulation developed by Criesfield leads to the following relationship between variation of global internal forces $\delta\mathbf{q}_i$ and variation of global displacement $\delta\mathbf{p}$,

$$\delta\mathbf{q}_i = (\mathbf{K}_{t1} + \mathbf{K}_{t\sigma})\,\delta\mathbf{p} \ , \tag{3}$$

where $\mathbf{K}_{t1}$ is the standard tangent stiffness matrix, $\mathbf{K}_{t\sigma}$ the geometric stiffness matrix. $\mathbf{K}_{t1}$ and $\mathbf{K}_{t\sigma}$ are displacement-dependent matrices.

In order to allow a sufficiently fine representation of tapering, the bow stick is discretized into 20 beam elements. The head is represented by a single element with diameter 10 mm, so as to make it sufficiently stiff. After assembling, the problem to solve takes the form:

$$\mathbf{K}(\mathbf{u})\,\mathbf{u} = \mathbf{f}(\mathbf{u}) \ , \tag{4}$$

where $\mathbf{u}$ is the displacement vector, $\mathbf{K}(\mathbf{u})$ the assembled stiffness matrix and $\mathbf{f}(\mathbf{u})$ the external force vector. The only external force in $\mathbf{f}(\mathbf{u})$ is the force $\mathbf{T}$ exerted by the hair on the stick at the tip [see Fig. 2(c)], which varies in orientation and amplitude in function of the displacement of the tip. The variation in orientation is due to the rotation of the hair coordinate system. The variation in amplitude is due to the increase in hair tension $\Delta T = T - T_0$ as the tip moves away from its position at T_0. Since $\mathbf{K}(\mathbf{u})$ and $\mathbf{f}(\mathbf{u})$ are displacement-dependent, an iterative procedure is necessary to solve Eq. (4). Moreover, an additional stiffness term for the last element, i.e. the head, has to be introduced to take into account the variation in force orientation and amplitude between two successive configurations. The additionnal stiffness term is expressed in a similar way as when follower forces are involved[22].

For the general case where the solution of the tightened and loaded bow is seeked, the numerical procedure achieves good convergence when decomposing the computation into two global load steps:

1. tightening of the bow, i.e. $T_x = T_0$ and $T_y = 0$,

2. loading of the hair, i.e. $T_x = T_0 + \Delta T_x$ and $T_y \neq 0$,

where T_x and T_y denote the components of $\mathbf{T}$. For both steps, the Newton-Raphson algorithm with several load increments is applied to reach the equilibrium.

Regarding the first step, a backward displacement of the frog relative to the stick (typically 3-3.5 mm) is normally needed to tighten a bow. This displacement counterbalances the stretching of the hair (1 mm) and the decreasing distance between the frog and the tip (2-2.5 mm) due to straightening of the stick and rotation of the head, as reported by Pitteroff[14]. In the model, neither the stretching of the hair at this step, nor the displacement of the frog is considered. Therefore, the distance between the frog and the tip decreases when tightening the modeled bow, whereas it slightly increases on an actual bow, because of the elongation of the hair. Although the increase in bow length is not fully negligible, it does not affect the overall behavior examined in the second step. Once the bow is tightened, the distance between frog and tip defines the hair length L_0 corresponding to tension T_0. In order to compute the value of T_x and T_y to apply in the second load step, a model of the hair is now defined.

C. Model of the hair

The ribbon of hair is assumed to behave like an equivalent single hair, represented in Figure 4. When an external force $\mathbf{F}$ is applied at relative abscissa γ ($0 < \gamma < 1$), the hair on either side is assumed to extend proportionally to the increase in tension $\Delta T = T - T_0$, where T is supposed to be the same on either side, i.e. $T = ||\mathbf{T}|| = ||\mathbf{T}'|| = \sqrt{T_x^2 + T_y^2}$. This implies that the force $\mathbf{F}$ has a small tangential component F_x of unknown value (except for $\gamma = 0.5$ where it is null).

It has to be noted that the distribution of forces in the x and y directions, respectively, is slightly different under normal playing conditions. In this situation, the tangential component of $\mathbf{F}$ corresponds to the friction force, i.e. $F_x = \mu\, F_y$, where the coefficient of friction μ varies within each cycle of Helmholtz motion[23,24]. As the force $\mathbf{F}$ is fully determined, the tension may differ on either side of bowing point. Cremer[1] reported a value of 0.24 for the

average coefficient of friction. With a typical bow force of 1 N, the corresponding average friction force is fairly small compared to hair tension. Thus, the difference between $||\mathbf{T}||$ and $||\mathbf{T}'||$ is likely to remain small, which gives support to the hypothesis made here.

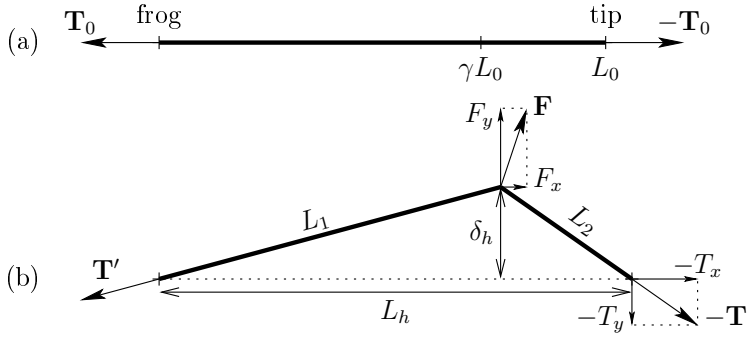

FIG. 4. Model of the hair. Tightened hair (a), deflection under loading (b).

The lengths of both sides are:

$$\begin{aligned} L_1 &= \gamma\, L_0\, (1 + c_h\, \Delta T) \\ L_2 &= (1 - \gamma)\, L_0\, (1 + c_h\, \Delta T) \ , \end{aligned} \tag{5}$$

where c_h is the compliance per unit length of the equivalent single hair. Considering a ribbon of n_h hairs having identical and homogeneous Young's modulus E_h and diameter d_h, an estimation of c_h can be obtained from:

$$c_h = \frac{4}{n_h\, E_h\, \pi\, d_h^2} \ . \tag{6}$$

Typical values for a violin bow are n_h = 160-190, E_h = 4-7 GPa and $d_h = 0.2 \pm 0.05$ mm, as reported by Askenfelt[6]. He also measured the stiffness constant of a complete ribbon and found it to reach 30 N.mm^{-1} under a nominal tension of 60 N. With a length $L_h = 650$ mm, the corresponding compliance per unit length is $c_h = 5.1 \times 10^{-5}$ N^{-1}.

The hair deflection at the loading point is

$$\delta_h = L_2\, \frac{T_y}{T} \ . \tag{7}$$

The distance between frog and tip is

$$L_h = \sqrt{L_1^2 - \delta_h^2} + \sqrt{L_2^2 - \delta_h^2} \ . \tag{8}$$

At this point, it can be shown that the normal component of $\mathbf{T}$ at the tip is simply given by

$$T_y = \gamma\, F_y \ . \tag{9}$$

The tangential component cannot be expressed by a similar equation. Therefore, it is found iteratively, starting from the initial guess $T_x = T_0$. At each computation step of the Newton-Raphson algorithm, the value of L_h is computed from Eq. (8) and compared to the distance between frog and tip in the current configuration. As long as the two values differ, the value of T_x is corrected for the next iteration.

D. Validation of the model

In this section, the ability of the finite element model to reproduce the deformed shape of an actual bow is examined. A wooden student violin bow was tightened from zero to high playing tension, by steps of two turns of the button. At each level, the shape of the stick was determined from a picture, by means of image processing [Fig. 5(a-c)]. The resolution in the measurement was about 0.3 mm. To keep the imaging conditions as identical as possible for all pictures, the position of both the bow and the camera were held constant. The diameter along the stick was measured with a digital caliper. The relative incertitude on the diameter was less than 3%. The Young's modulus was then determined from two measurements of the dynamic response of the stick simply supported at its ends and loaded by a mass at its center (200 g and 400 g), by means of the measuring platform *Lutherie tools*[25]. A value of 36 GPa was found.

Then, simulations were performed starting from the initial geometry. For each level of hair tension, the value of T_0 giving the best least-squares fit between measured shape and model output was determined. The maximum difference between the experimental and numerical results on the y-coordinate of the neutral axis was less than 0.2 mm. It should be noted that this procedure can be considered as an indirect measurement of hair tension, provided that the Young's modulus is known. With the bow used in this experiment, values of T_0 = 20.1 N, 39.2 N, 54.9 N and 67.5 N (resp. at 2, 4, 6 and 8 turns of the button)

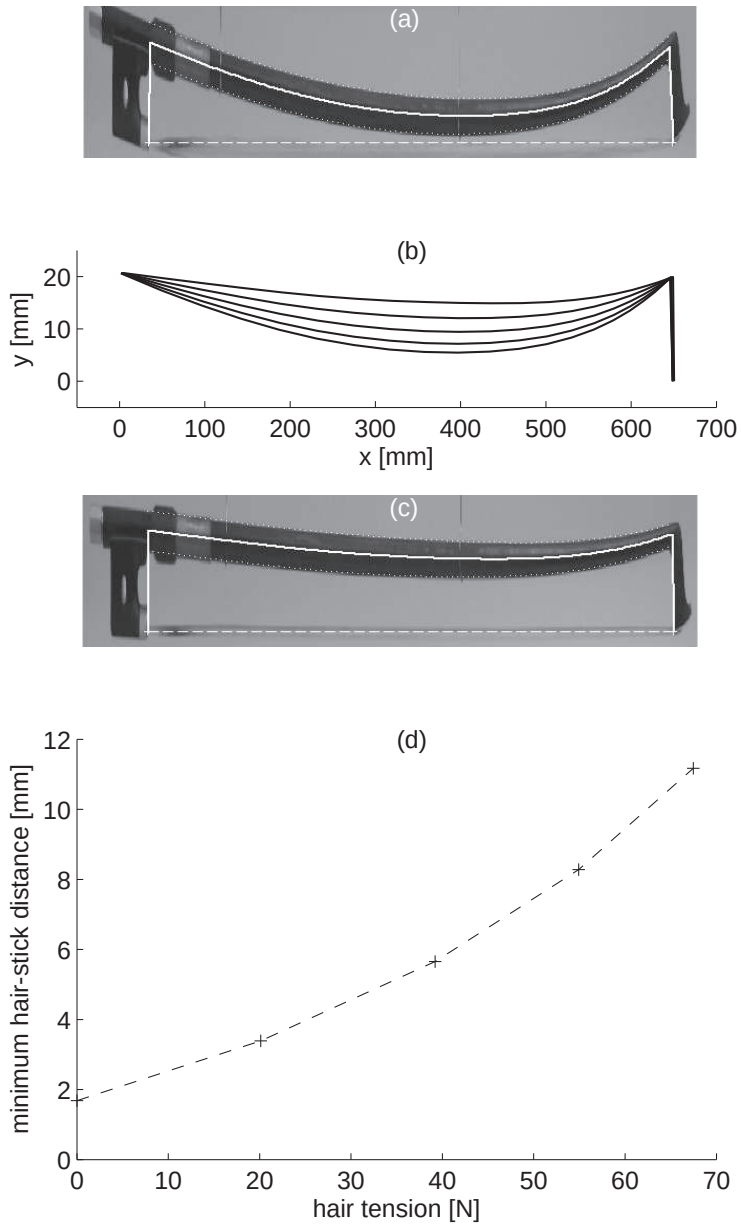

FIG. 5. Bow used for validating the model. (a) Initial measured shape. (b) Successive shapes of the bow from zero tension to high playing tension, by steps of two turns of the button. The y-coordinate indicates the distance from the level of the bow hair to the neutral axis of the stick. (c) Final measured shape. (d) Estimated hair tension T_0 at each level vs. minimum hair-stick distance.

were obtained. The levels of hair tension corresponding to 4 and 8 turns of the button were considered as the lower and upper limits for playing, respectively. The optimal playing

tension was found at 6 turns ($T_0 = 54.9$ N). Although a typical value of 60 N is commonly refered to as "normal" playing tension by authors[14,26,27], the optimal value for each bow probably depends on the stiffness of the stick and camber as well. Figure 5(d) shows the nonlinear increase in minimum hair-stick distance with hair tension.

III. RESULTS

In this section, we first describe the geometry of a "standard bow" on which simulations are performed. Then, general results from simulations are presented and discussed with respect to experimental observations by other authors. Finally, the influence of initial hair tension and camber on transverse bow compliance is examined.

A. Definition of a standard bow

The geometry of the modeled stick, which is basically defined by camber and tapering, can be taken from measurements on a representative modern violin bow. In this study, however, we define the geometry of a "standard bow" from criteria found in the literature. Similarly, the Young's modulus E is fixed at 25 GPa, which is a typical value for pernambuco[15,28,29]. Measurements of a set of bows in professional use today would be needed to check whether this "standard bow" is representative of most bows available on the market.

1. Tapering

The tapered profile is derived from a formula given by Vuillaume. This violin maker of the 19th century measured a great number of Tourte bows and found the diameter to decrease logarithmically along the stick[30]. The corresponding curve is considered as a reference in some studies[4,31]. The original formula applies to abscissa between 110 mm and 700 mm from the stick origin and corresponds to a decrease in diameter from 8.6 mm to 5.3 mm, the first 110 mm of the stick having constant diameter of 8.6 mm. Since the origin of the modeled bow is the front end of the frog, the formula is adapted so that it applies to abscissa between

0 mm and 650 mm, neglecting the small portion of constant diameter [Fig. 6(a)]. Thus, the diameter d at abscissa x is given by:

$$d(x) = d_0 \left(1 + \varepsilon \, \ln\!\left(\frac{x_\infty - x}{x_\infty}\right)\right) \ , \tag{10}$$

where $d_0 = 8.77$ mm, $x_\infty = 825$ mm and $\varepsilon = 0.255$. Interestingly, the second moment of inertia $I(x)$ following from Eq. (10) decreases almost linearly with abscissa for this set of parameters. It can be approximated by

$$I(x) \approx I_0 \left(\frac{x - x_0}{x_0}\right) \ , \tag{11}$$

where $I_0 = 293$ mm^4 and $x_0 = 752$ mm, with 3% maximum relative difference with that deduced from Eq. (10). Since this observation has no obvious physical interpretation, one may wonder whether this particular tapered profile is an optimum empirically found by Tourte.

2. Camber

The concept of camber actually includes two aspects: distribution of camber, which can be seen as shape of the stick; amount of camber, which represents how strong the stick is bent. The distribution of camber is here defined so that the stick becomes straight under a certain tension, which is a criteria commonly recognized by bow makers: "The match between wood strength and camber can be tested by tightening the bow until the stick is straight (...) If the stick is really straight, camber and wood strength are properly matched" (Grütter[19]); "One reference: the axis of the stick should be perfectly parallel to the line of hair at maximum tension of the bow" (Rolland[20]). The maximum tension, i.e. the tension at which the stick is straight, is denoted by $T_0^{\max}$. In this configuration, the distance between hair and neutral axis of the stick is constant [Fig. 6(b)], assuming that the frog and the head have the same height h. Thus, the bending moment resulting from hair tension has a constant value $\mathcal{M}_0^{\max} = h\, T_0^{\max}$ along the stick. Therefore, neglecting axial compression of the stick as well as deformation of the head, the initial curvature of the stick

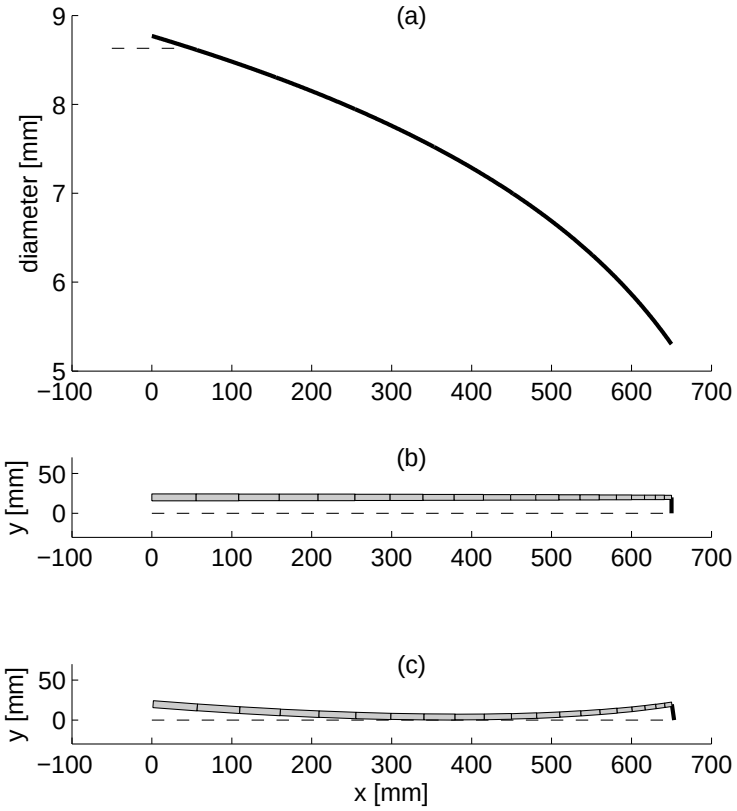

FIG. 6. Geometry of the standard bow. (a) Tapering, - - after Vuillaume[30], — from Eq. (10). (b) Straight stick. (c) Cambered stick showing the case of a "full camber".

can be determined by calculating the deformed shape of the initially straight stick subject to moment $\mathcal{M}_0^{\max}$ at its free end [Fig. 6(c)].

Following this reasoning and considering the approximation of Eq. (11), a simple analytical expression giving the initial shape of the stick $y(x)$ can be provided by integrating $\dfrac{d^2y}{dx^2} = \dfrac{h\,T_0^{\max}}{E\,I(x)}$ (with $y(0) = h$ and $y'(0) = 0$), which yields

$$y(x) - h = \frac{h\,T_0^{\max}\,{x_0}^2}{E\,I_0}\big(\bar{x} + (1-\bar{x})\,\ln(1-\bar{x})\big)\ , \tag{12}$$

where $\bar{x} = \dfrac{x}{x_0}$. The multiplying factor in Eq. (12), in terms of E, I_0, and $T_0^{\max}$, is considered to be the amount of camber. The expression within the parentheses, dependent on $\bar{x}$, gives the generic shape of the stick without hair tension (distribution of camber).

For a given bow, the maximum tension $T_0^{\max}$ is the input parameter that determines the amount of camber of the modeled stick. Althought it corresponds to a physical quantity, a more convenient way of quantifying the amount of camber is the minimal distance between loosened hair and stick, denoted by κ. The smaller this distance, the more camber the stick has. It is generally agreed among bow makers that this distance should be between 0 mm and 2 mm and in any case not negative. The case where $\kappa = 0$ mm is called "full camber". In this study, four different amounts of camber are investigated. The value of $T_0^{\max}$ needed to obtain each chosen value of κ is determined by means of the finite element model. The corresponding values of κ and $T_0^{\max}$ are listed in Table I.

3. Comment on the relationship between tapering and camber

In playing conditions, the bow is never tightened up to complete straightening of the stick. Therefore, the bending moment resulting from hair tension is a function of abscissa x, $\mathcal{M}_0(x) = T_0\, a(x)$, where a denotes the distance between hair and neutral axis of the stick. It is maximum at the tip and at the frog (both head and frog have standard height on modern bows) and minimum at the lowest point of the stick, generally near the middle. Moreover, the stiffness of the stick is determined by the quantity $E\,I$, where Young's modulus E is supposed to be homogeneous along the stick, contrary to second moment of inertia I which depends on tapering. For a circular section, $I = \dfrac{\pi\, d^4}{64}$. Thus, the stick is far more compliant at the tip than at the frog. The local bending radius ρ that counteracts the initial curvature of the stick is given by:

$$\frac{1}{\rho} = \frac{\mathcal{M}_0}{E\,I}\ . \tag{13}$$

From Eq. (13) it is clearly apparent that the stick will bend more near the tip, where the bending moment is maximum and the stiffness minimum. For this reason, camber is particularly strong in the last portion of the stick. More generally, the role of distribution of camber is to compensate for the decrease in diameter along the stick. In addition, the more cambered the stick, the less it will straighten under the same tension. Since tapering is

mostly adjusted so that the stick reaches a given mass, the bow maker has to adjust camber accordingly, in order to get the right shape on the tightened bow. A physical model can be useful to determine the proper camber for a given tapering, as pointed out by a recent study[32].

B. Variation in hair tension under transverse loading

In previous studies on violin bows, the influence of hair tension on different properties of the bow, e.g. bending stiffness along the stick[6], stick mode frequencies[7], bouncing frequency[26], has been examined. In most studies, the hair tension has been assumed not to vary significantly from the initial value fixed by the player before playing. However, it has been experimentally shown by Demoucron *et al.*[27] that the hair tension does vary when the bow is loaded by a normal force. The tension variation was found to be almost linear with respect to relative abscissa γ and normal force F_y, leading to a simple empirical relation,

$$T = T_0 + \alpha_T \, \gamma \, F_y \ , \tag{14}$$

where α_T is an experimentally determined coefficient.

Figure 7 shows the simulated hair tension variation when the bow is loaded by a normal force F_y of increasing value at relative abscissa γ. The tension increases almost linearly with relative abscissa and normal force, which is in agreement with the observations of Demoucron. For a normal force of 1.5 N at the middle and 1.0 N at the tip, which are moderate values in violin playing, the hair tension increases by 20% and 25%, respectively. For a normal force of 1.5 N at the tip, it increases by 40%. As a comparison, Demoucron measured a variation of 25% for the same load case. This discrepancy could be due to the higher stiffness of the bow he used for the experiment (stiffness at the tip $K_s = 91$ N.m^{-1}) compared to the modeled bow ($K_s = 72$ N.m^{-1}), since the increase in hair tension is essentially due to the displacement of the tip under loading.

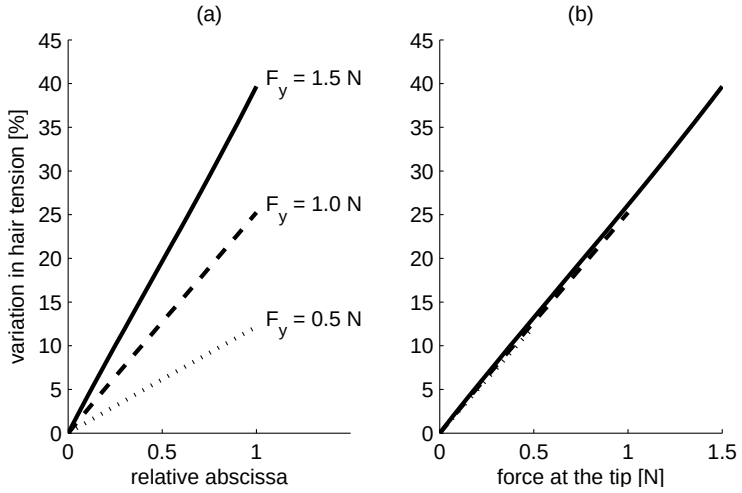

FIG. 7. Variation in simulated hair tension for three values of normal force F_y (0.5 N, 1.0 N and 1.5 N) applied at different places along the bow hair, shown as function of (a) relative abscissa γ, and (b) force at the tip $\gamma\, F_y$. The simulations are performed on the standard bow with full camber. The initial hair tension T_0 is fixed at 45.0 N, which corresponds to 10 mm hair-stick distance.

C. Distribution of transverse compliance along the bow

When applying a normal force to the tightened bow hair, the observed deflection at the loading point is the result of two effects: deflection of the hair and bending of the stick. The force transmitted by the hair to the tip makes the stick bend. This results in a second displacement term, in addition to the hair deflection.

Pitteroff[14] considered the two effects separately to give an analytical relationship between force and deflection. The contribution of the hair was the deflection δ_h of a string with fixed length L_h and tension T_0 under normal force F_y at relative abscissa γ. The contribution of the stick was deduced from the deflection δ_s of a cantilever beam under normal force γF_y at its free end. The stick was assumed to be straight and have constant bending stiffness. However, the formula remains valid when considering a more realistic geometry, simply by introducing the equivalent stiffness constant at the tip K_s[27]. The total deflection at the

loading point was expressed as the sum of the two contributions:

$$\delta = \delta_h + \delta_s = \frac{\gamma(1-\gamma)L_h}{T_0}F_y + \frac{\gamma^2}{K_s}F_y \ . \tag{15}$$

When compared to experimental results, this relationship matched well with the behavior of an actual bow in its lowest two thirds. However, a significant difference between experimental and theoretical deflection was observed at the tip.

The model developed in the present article removes the hypothesis that the effects of hair and stick are uncoupled. Yet, it is possible to estimate how hair and stick contribute to the total deflection. The hair deflection is given by Eq. (7). The total deflection is deduced from coordinates of the loading point before and after the force is applied. The contribution of the stick is then given by the difference between total deflection and hair deflection.

Figure 8 shows the simulated total deflection at the loading point of the standard bow loaded by a 1 N normal force plotted against relative abscissa of the force. Hair and stick contributions are also plotted individually. The total deflection is null at the frog and maximum at the tip. The stick deflection continuously increases along the bow, reaching a maximum at the tip. On the contrary, the shape of the hair contribution is similar to a parabola, though it is slightly asymmetrical: the maximum value is reached just before the midpoint of the bow. This asymmetry is due to the rise in hair tension with relative abscissa.

As a comparison, it is possible to estimate the parameters T_0 and K_s used by Pitteroff by fitting the total deflection with a second order polynomial of the same form as Eq. (15) and identifying the coefficients. The third parameter, L_h, is known from the finite element model. From this method, the estimated value of hair tension is found to be 24% higher than its actual value, $T_0 = 45.0$ N. The same operation was done for three other values of F_y. The estimated values for T_0 and K_s, as well as the maximum relative difference in deflection between numerical results and the second order polynomial, are given in Table II. Regarding the hair tension, the deviation from actual value increases with force F_y. Similarly, the estimated value of K_s varies significantly with F_y. This shows that Eq. (15) does not

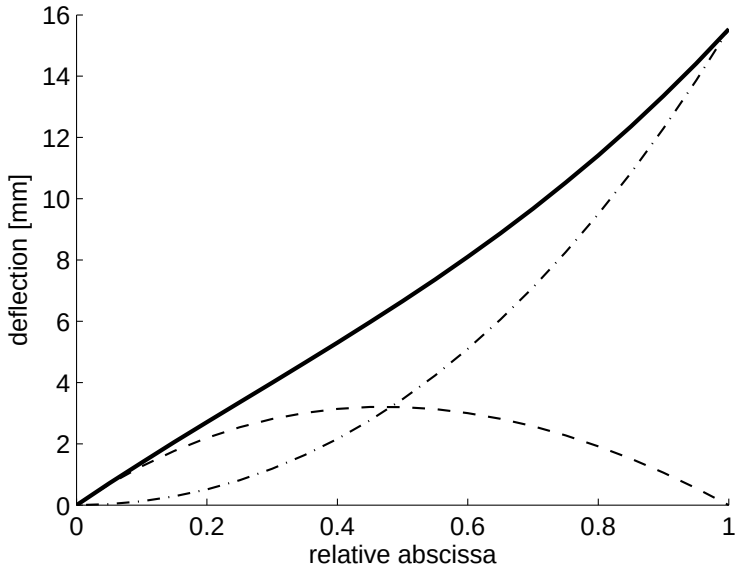

FIG. 8. Evolution of deflection at the loading point vs. relative abscissa for applied normal force $F_y = 1$ N. — total deflection, - - hair deflection, -·- stick deflection. Standard bow with full camber, initial hair tension $T_0 = 45$ N.

reflect exactly the behavior of the bow.

Moreover, Pitteroff observed that the transverse compliance of the bow varies with the normal force. In the lower half, the measured compliance was lower with a higher force (5 N compared to 1 N). On the contrary, the compliance near the tip increased with the force. The nonlinearity of transverse compliance close to the tip was also reported by Askenfelt[6]. Figure 9 shows the simulated deflection of the bow as a function of normal force at three different loading points. The normal force F_y is limited to the range between 0 N and 1.5 N. Although the bow force generally remains low when playing near the tip, it may well reach values around 1.5 N in this part of the bow[33]. A comparison with a linear case, indicated by dotted lines in Figure 9 can be made. As seen, the simulated transverse compliance is nonlinear. Close to the frog as well as in the middle, the compliance tends to diminish as the force increases. This is due to the increase in hair tension with force. Near the tip, the compliance increases with the force.

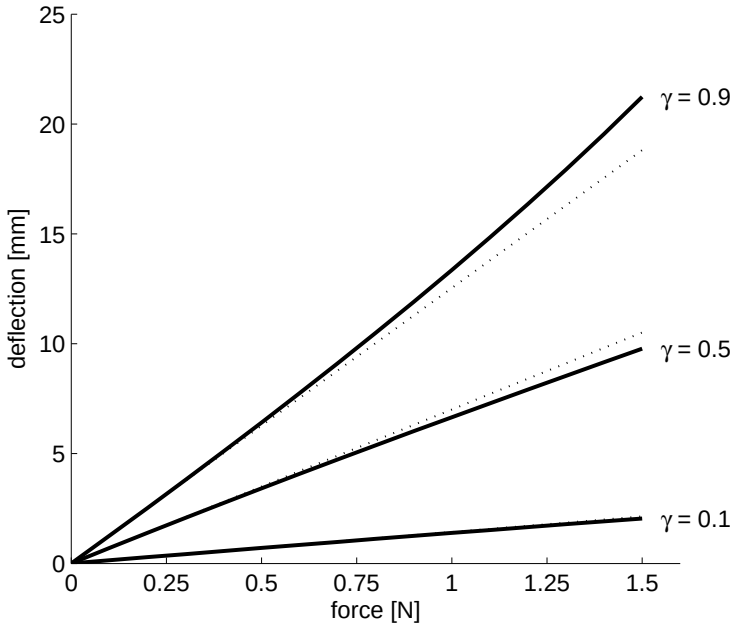

FIG. 9. Evolution of transverse bow deflection at the loading point vs. normal force for three values of relative abscissa. The deviation from a linear evolution (dotted lines) indicates a nonlinear transverse compliance.

D. Influence of initial hair tension on transverse compliance

Before playing, the player adjusts the initial hair tension by turning the button. As the tension increases, the stick straightens progressivly, which increases the minimum distance between hair and stick. The evolution of minimum hair-stick distance with tension for four settings of camber (4 mm, 2 mm , 0 mm and -2 mm) is plotted in Figure 10. The increase in hair-stick distance with tension is far from linear. This is due to the fact that the straightening of the stick, which increases the hair-stick distance, is the consequence of a bending moment which itself depends on the hair-stick distance.

To evaluate the influence of initial hair tension on the transverse compliance of the bow, simulations were performed for four values of T_0 on the standard bow with full camber. The values of T_0 (40.5 N, 45.2 N, 49.0 N, and 52.1 N) correspond to four plausible values of hair-stick distance, from 8 mm to 14 mm, denoted by numbers (0) to (3) in Figure 10. Because of nonlinearity, the transverse compliance depends on normal force. It is defined

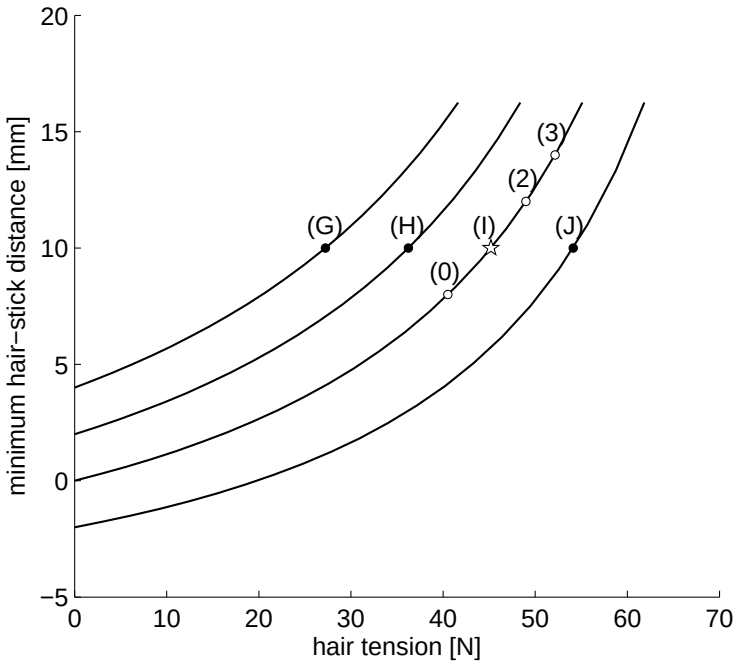

FIG. 10. Evolution of minimum hair-stick distance vs. hair tension for four settings of camber (4 mm, 2 mm , 0 mm = full camber and −2 mm). Points denoted by letters (G) to (J) represent playing tension T_0^{play} for each camber giving a bow-hair distance of 10 mm. Points denoted by numbers (0) to (3) indicate four settings of hair tension for the case of full camber with (I) as a common reference. Note that rightmost curve represents negative camber, meaning that the middle of the stick is below the level of the bow hair before tightening.

by the slope of the force-deflection curve (see Fig. 9).

Figure 11 shows the transverse compliance along the bow with full camber corresponding to the four chosen values of initial hair tension. For each setting, the two curves indicate the compliance for small forces (just above 0 N) and high forces (around 1.5 N). The compliance for small forces slightly decreases with initial hair tension. Increasing T_0 from 40.5 N to 52.1 N (29%) lowers the compliance for small forces at the middle of the bow by 18% and by 13% at the tip. Moreover, the nonlinearity is stronger for a low hair tension.

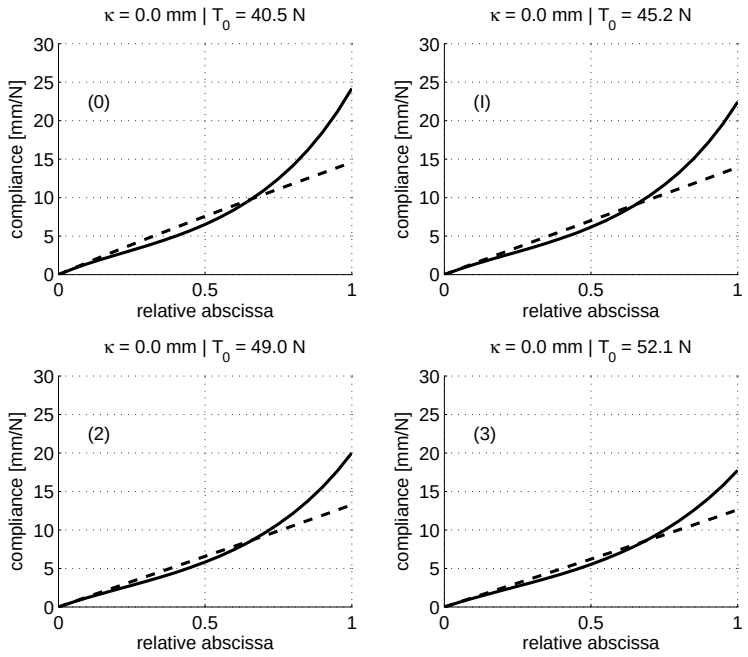

FIG. 11. Transverse compliance along the standard bow with full camber for four settings of initial hair tension T_0, for two normal forces: around 0 N (- -) and 1.5 N (—). The four cases correspond to points (0) - (3) in Figure 10.

E. Influence of camber on transverse compliance

When varying camber in the model, it is necessary to change the initial hair tension accordingly so that the minimum hair-stick distance remains in a range which is suitable for playing. For each setting of camber in Figure 10, the tension at which a 10 mm hair-stick distance is reached is denoted by T_0^{play} and called "playing tension". Figure 10 shows the four settings of camber, denoted by letters (G) to (J). Table I gives the corresponding values of κ, T_0^{play} and tension for straight stick $T_0^{\max}$. None of the different settings of camber and hair tension led to contact between hair and stick within the chosen ranges of relative abscissa and normal force.

The first noticeable effect of camber is a change in playing tension. Increasing camber from $\kappa = 4$ mm up to $\kappa = 0$ mm, for example, increases the hair tension by 66% for the same hair-stick distance. It is noteworthy that not only the minimum hair-stick distance is

preserved, but also the hair-stick distance throughout the bow. Thus, the bow maker can increase the playing tension of a bow without any consequence on its shape once tightened.

A second effect of camber is a change in transverse compliance (see Fig. 12). As camber increases, the compliance at small forces decreases in the middle (-22% from $\kappa = 4$ mm to 0 mm), which is due to a higher playing tension. At the tip, the compliance at small forces increases with camber ($+10\%$ from $\kappa = 4$ mm to 0 mm), contrary to what was observed by increasing the hair tension at given camber (Fig. 11). This effect is due to prebending of the stick.

Furthermore, if the bow is not cambered very much (G), the nonlinearity is fairly strong around the middle: the higher the force, the lower the compliance. Close to the tip, the reverse trend is observable though moderate. As camber increases, the nonlinearity tends to decrease around the middle of the bow, whereas it increases near the tip. At full camber (I), the compliance in the lower two-thirds is almost the same for small and high forces, whereas the compliance near the tip significantly increases with force. Moreover, the range in length for which the compliance increases with force becomes larger as camber increases. If the bow has an unrealistically large amount of camber (negative κ, point J), the compliance for high forces strongly increases in the last third.

IV. CONCLUSION

A finite element model of the assembled bow accounting for the geometrical nonlinearity of both stick and hair has been presented. The model allows to reproduce the in-plane nonlinear static behavior that is experimentally observed when the bow is loaded (Fig. 2). The influence of the adjusting parameters (camber, hair tension) on the mechanical behavior of the bow has been enlightened. Changing the hair tension does not affect the overall profile of the transverse compliance of the bow. However, increasing the hair tension tends to reduce the nonlinearity. On the contrary, different amounts of camber lead to very different profiles of the compliance along the bow. The nonlinearity of the compliance near the tip is especially

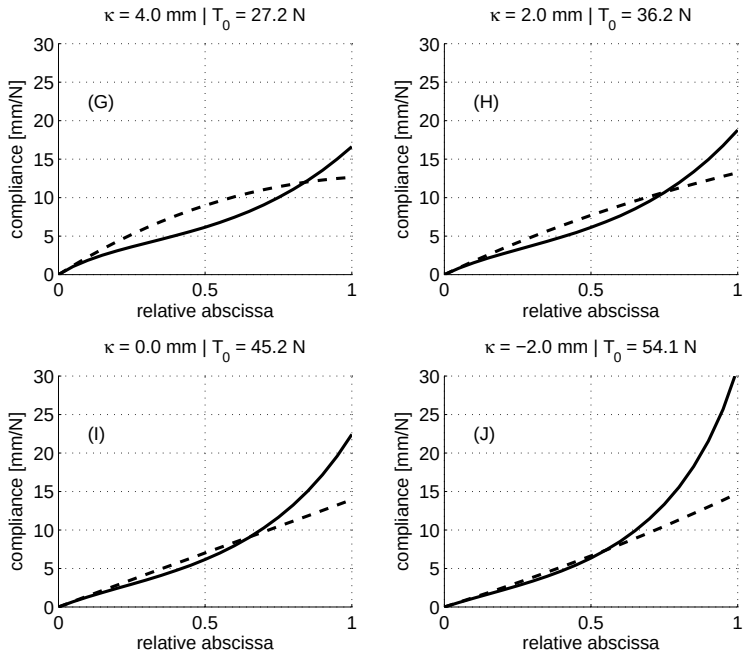

FIG. 12. Transverse compliance along the bow for different settings of camber (characterized by minimal hair-stick distance without hair tension $\kappa = 4$ mm, 2 mm, 0 mm and -2 mm) and playing tension T_0^{play}, for two normal forces: around 0 N (- -) and 1.5 N (—).

apparent with increasing camber.

It remains to be seen if results from this study have direct applications in predicting a player's perception of bow performance. Compliance is generally assumed to be of particular importance for bow force control: if too low, the bow might be too sensitive to small variations of hand movement; if too high, the bow would not be responsive enough[6]. Measurements and playing tests of bows with different settings of camber and hair tension will be performed to go deeper into this question. If significant trends emerge, the model presented in this paper would be useful to assist bow makers. Furthermore, since the bow is often tilted towards the fingerboard in playing[34,35], a model based on spatial beam elements is currently developed in order to take into account the out-of-plane bending of the stick.

Acknowledgments

The study presented in this paper was partially supported by the French National Research Agency (ANR) within the PAFI project. The authors wish to thank two anonymous reviewers for helpful comments on a previous version of this manuscript, and Matthew Boucher for his careful reading of the manuscript.

References

[1] L. Cremer, *The physics of the violin*, 474 p. (MIT Press, Cambridge, 1984).

[2] C. Hutchins and V. Benade, eds., *Research papers in violin acoustics: 1975-1993*, 1312 p. (Acoustical Society of America, Woodbury, 1997).

[3] R. Schumacher, "Some aspects of the bow", Catgut Acoustical Society Newsletter **24**, 5–8 (1975).

[4] N. Pickering, "Physical characteristics of violin bows", Journal of the Violin Society of America **8**, 41–58 (1987).

[5] A. Askenfelt, "A look at violin bows", STL-QPSR **34**, 41–48 (1993).

[6] A. Askenfelt, "Observations on the violin bow and the interaction with the string", STL-QPSR **36**, 23–42 (1995).

[7] R. Caussé, J.-P. Maigret, C. Dichtel, and J. Bensoam, "Study of violin bow quality", in *International Symposium on Musical Acoustics*, Perugia, Italy, 1–6 (2001).

[8] N. Dauchez, J.-M. Génevaux, and I. Brémaud, "Qualité des archets de violon et instabilité de type flambement" (Quality of violin bows and buckling instability), in *8e Congrès Français d'Acoustique*, Tours, France, 459–462 (2006).

[9] E. Ravina, P. Silvestri, and A. Airenti, "Experimental modal analysis of bows", in *Acoustics'08*, Paris, France, 4833–4838 (2008).

[10] T. Rossing, ed., *The science of string instruments*, chapter "Bows, Strings, and Bowing", 279–299 (Springer, New-York, 2010).

[11] K. Guettler and A. Askenfelt, "Some aspects of bow resonances – conditions for spectral

influence on the bowed string", STL-QPSR **36**, 107–118 (1995).

[12] B. Rolland, "Sticking point", The Strad **114**, 614–619 (2003).

[13] U. Wegst and M. Ashby, "Alternative woods for violin bows", Newsletter of the British Violin Making Association 7–13 (1996).

[14] R. Pitteroff, "Contact mechanics of the bowed string", Ph.D. thesis, University of Cambridge, UK (1995).

[15] P. Carlsson and M. Tinnsten, "Geometrical compensation for varying material properties in bows by the use of numerical optimization", Acta Acustica united with Acustica **93**, 145–151 (2007).

[16] A. Mamou-Mani, J. Frelat, and C. Besnainou, "Numerical simulation of a piano soundboard under downbearing", J. Acoust. Soc. Am. **123**, 2401–2406 (2008).

[17] F. Ablitzer, N. Dauchez, J.-P. Dalmont, and N. Poidevin, "Mécanique de l'archet de violon : lien entre évolution et répertoire musical" (Mechanics of the violin bow: relationship between evolution and musical repertoire), in *5th Conference on Interdisciplinary Musicology*, Paris, France, 1–7 (2009).

[18] N. Poidevin, "Premiers archets à travers l'iconographie" (Early bow in iconographic sources), Musique & Technique **4**, 109–124 (2009).

[19] A. Grütter, "A bow on the couch", URL `http://www.andreasgrutter.nl/` (last viewed 10 March 2011).

[20] B. Rolland, "The playing parts of the bow: focusing on the stick", Journal of the Violin Society of America **19**, 201–217 (2002).

[21] M. A. Crisfield, *Non-linear finite element analysis of solids and structures*, 201–233 (Wiley, Chichester, 1991).

[22] J. Argyris and H.-P. Mlejnek, *Dynamics of structures*, 527–561 (North-Holland, Amsterdam, 1991).

[23] R. T. Schumacher, "Measurements of some parameters of bowing", J. Acoust. Soc. Am. **96**, 1985–1998 (1994).

[24] J. Woodhouse, R. T. Schumacher, and S. Garoff, "Reconstruction of bowing point friction

force in a bowed string", The Journal of the Acoustical Society of America **108**, 357–368 (2000).

[25] F. Gautier, V. Doutaut, and J.-M. Fouilleul, "*Lutherie tools* : projet collaboratif entre ateliers de lutherie et laboratoires" (*Lutherie tools*: a project between instrument makers and laboratories), Musique & Technique **4**, 21–28 (2009).

[26] A. Askenfelt, "Observations on the dynamic properties of violin bows", STL-QPSR **33**, 43–49 (1992).

[27] A. Demoucron, A. Askenfelt, and R. Caussé, "Measuring bow force in bowed string performance: Theory and implementation of a bow force sensor", Acta Acustica united with Acustica **95**, 718–732 (2009).

[28] M. Matsunaga, M. Sugiyama, K. Minato, and M. Norimoto, "Physical and mechanical properties required for violin bow materials", Holzforschung **50**, 511–517 (1996).

[29] L. Schimleck, C. Espey, C. Mora, R. Evans, A. Taylor, and G. Muniz, "Characterization of the wood quality of pernambuco (*Caesalpinia echinata* lam) by measurements of density, extractives content, microfibril angle, stiffness, color, and NIR spectroscopy", Holzforschung **63**, 457–463 (2009).

[30] F.-J. Fétis and J. Bishop, *Notice of Anthony Stradivari, the celebrated violin-maker, known by the name of Stradivarius*, chapter "Experimental determination of the form of Tourte's bows", 121–124 (R. Cocks and co., London, 1864).

[31] R. Hopfner, "Zur Entwicklung des Streichbogens anhand von Objekten der Sammlung alter Musikinstrumente, Wien" (Evolution of the bow in a collection of old musical instruments), in *16. Musikinstrumentenbau-Symposium*, Michaelstein, Germany, 57–74 (Stiftung Kloster Michaelstein, 1998).

[32] J. Graebner and N. Pickering, "Optimizing the taper-camber relationship in bows for string instruments. (a)", J. Acoust. Soc. Am. **127**, 1791–1791 (2010).

[33] A. Askenfelt, "Measurement of bow motion and bow force in violin playing", J. Acoust. Soc. Am. **80**, 1007–1015 (1986).

[34] E. Schoonderwaldt, "Mechanics and acoustics of violin bowing: Freedom, constraints and

control in performance", Ph.D. thesis, Royal Institute of Technology (KTH), Stockholm, Sweden (2009).

[35] E. Schoonderwaldt and M. Demoucron, "Extraction of bowing parameters from violin performance combining motion capture and sensors", J. Acoust. Soc. Am. **126**, 2695–2708 (2009).

TABLE I. Standard bow. Relationship between amount of camber, characterized by minimum hair-stick distance κ, and maximal tension $T_0^{\max}$ (tension for straight stick). Corresponding values of playing tension T_0^{play} (tension for 10 mm hair-stick distance) are given.

κ (mm)	$T_0^{\max}$ (N)	T_0^{play} (N)
4.0	41.6	27.2
2.0	48.4	36.2
0.0	55.1	45.2
−2.0	61.8	54.1

TABLE II. Standard bow with full camber. Estimated values of T_0 and K_s [see Eq.(15)] from simulation with the finite element model, for different values of normal force F_y. The last column gives the maximum relative error between numerical simulations of the deflection and fitted curve.

F_y (N)	T_0 (N)	K_s (N.m^{-1})	max error (%)
0.1	46.1	72	2
0.5	49.9	70	8
1.0	56.1	66	17
1.5	65.5	61	27

List of Figures